RSC Advances

PAPER

View Article Online
View Journal | View Issue

Cite this: *RSC Adv.*, 2018, **8**, 26255

Synthesis and properties of novel ammonium-based room-temperature gemini ionic liquids†

Xuzhao Yang [ab] and Yun Fang *[a]

Received 15th May 2018
Accepted 3rd July 2018

DOI: 10.1039/c8ra04127j

rsc.li/rsc-advances

Ammonium-based room-temperature asymmetrical gemini ionic liquids, 1-trimethylammonium-3-(pyridinium) propane bisdicyanamide ($[N_{111}C_3Py][DCA]_2$) and 1-trimethylammonium-3-(1-methylpiperidinium)propane bisdicyanamide ($[N_{111}C_3MPi][DCA]_2$) were respectively synthesized and structurally characterized by ^{1}H NMR and ^{13}C NMR. Thermal stability of the gemini ionic liquids was determined by thermogravimetric analysis under a pure nitrogen atmosphere. Densities and viscosities of pure GILs and their binary mixtures with acetonitrile (MeCN) were investigated over the entire range of mole fractions at various temperatures, from 288.15 to 333.15 K, under atmospheric pressure. Moreover, the excess molar volumes (V_m^E) and the viscosity deviations ($\Delta\eta$) of the binary mixtures were evaluated and well fitted to the Redlich–Kister polynomial expression. The negative values of V_m^E and $\Delta\eta$ result from strong self-association and interaction between the gemini ionic liquid molecules and MeCN. Results are discussed in terms of molecular interactions and structures.

1 Introduction

The pretreatment and transformation of biomass (such as lignocellulosic materials) remain a challenge owing to the complex structure of biomass. Biomass conversion consists of a fair amount of chemical and biological processes which require suitable solvents for the dissolution of various biomass materials. It is difficult to dissolve biomass using traditional organic solvents. Environmentally friendly and biocompatible solvents such as ionic liquids are preferred for use in the biorefining processes due to their unique performance in dissolving whole biomass or selected saccharides such as cellulose, hemicellulose, lignin, glucose and mannose.

Ionic liquids (ILs) consisting of only anionic and cationic species have been tailored as replacements for organics commonly used in reactions or separations in the academic and industrial fields due to their negligible volatility, non-flammability, thermal stability, wide electrochemical window, wide liquidus range, recyclability, and so on.[1–5] Their unique and tunable physicochemical properties such as melting point, density, viscosity, solubility, heat capacity and surface tension mainly depend on the possible cation and anion combinations. Each cation or anion is associated with an equivalent anion or cation that is either hydrophobic or hydrophilic, providing almost infinite opportunities to design desired ILs with functionalities to fit possible chemical processes and physical applications in materials science and technology.[6–9] To date, most investigated ILs are still traditional monocationic ILs. Most IL studies focus on synthesis, properties, the relationships between structure and properties, molecular dynamics, and applications.

Recently, other than the monocationic types, a novel category of ILs, namely gemini ILs (GILs), consisting two cationic head groups linked by a rigid or flexible spacer and two anionic moieties, have gained increasing attention due to their superior properties in terms of thermal stability, tunability and volatility.[10] The physicochemical properties such as melting point, density, viscosity, solubility, heat capacity, surface tension and solubility behaviors can thus be altered and engineered to a greater extent than the traditional ILs because of the larger number of possible combinations of numerous cationic moieties, anions, and linkages. Therefore, GILs have been proposed to serve as gas chromatography stationary phases,[11,12] solvents for high-temperature reactions,[13] and novel high-temperature lubricants[14] where conventional ILs fail. Some investigations in GILs have explored their specific and/or desired applications in the field of science and technology.

In the past few years, relatively little attention has been paid to GILs because of the much fewer reports compared with monocationic ILs, and the understanding on GILs is thus lacking. Part of the reason may be that GILs still possess some inconveniences and disadvantages. In some instances, GILs display higher melting points and viscosities in comparison with common monocationic analogues with the same anion. Sometimes, they present as solids even beyond 100 °C (ref. 15) and show higher viscosities even at high temperatures, which may result in decreasing rates of mass transfer and increasing

[a]The Key Laboratory of Synthetic and Biological Colloids, Ministry of Education, School of Chemical and Material Engineering, Jiangnan University, Wuxi 214122, China. E-mail: yunfang@126.com; yangxz@zzuli.edu.cn

[b]Henan Provincial Key Laboratory of Surface and Interface Science, School of Material and Chemical Engineering, Zhengzhou University of Light Industry, Zhengzhou 450002, China

† Electronic supplementary information (ESI) available. See DOI: 10.1039/c8ra04127j

pumping costs, thus limiting their real potential applications to the processes requiring higher temperatures. Some experimental and theoretical efforts to design and synthesize novel GILs with lower melting points and viscosities have been made while our work was in progress.[16,17] The most common methodology for lowering the melting point of GILs is to change the counteranions, which thus can alter the solvation properties. According to the literature on this subject, incorporating larger bulky or asymmetrical cationic moieties into the structure of GILs can reduce the cohesive forces and depress ion pairing. Meanwhile, GILs with longer alkane linkage tend to have comparatively lower melting points. As for GILs, it has been proven that employing the longer alkyl chains, introducing specified functional groups, or matching the relatively low symmetry, high flexibility, and weakly coordinating anions can decrease the viscosity. The combination of dicyanamide (DCA), bis(trifluoromethane)sulfonamide (NTf_2), or trifluoromethanesulfonate (TfO) anion with cations may form lower-viscosity GILs. Meanwhile, GILs possess the same desirable solvation properties and can dissolve various biomass materials. Therefore, another easy approach to decrease the dynamic viscosity at low temperatures and reduce the costs is to mix GILs with less viscous conventional organic co-solvents or other molecular liquids. The viscosities of pure GILs and their mixtures with other less viscous solvents are essential data, and the knowledge is primordial for industrial and academic processes.

When GILs are applied in academic and industrial fields, it is important to determine and understand their physicochemical properties, namely density, viscosity, thermal behavior, and the relationships between these properties and ionic species and structures. A systematic and precise evaluation of physicochemical properties may be equally important in academic research because it is the required beginning of a comprehensive study of GILs and can help us find optimum GILs for real applications. The accumulation of these data and relationships between the properties and structures may be also an essential step to designing and synthesizing desired GILs. Until now, the systematic and accurate knowledge of physical and chemical properties of GILs and their mixtures with molecular co-solvents are still very lacking compared with conventional monocationic ILs.

To our knowledge, GILs containing DCA anion possess lower melting points and dynamic viscosities due to the coordinating ability of this anion.[18–20] In the present work, novel unsymmetrical ammonium-based room-temperature GILs, 1-trimethylammonium-3-(pyridinium)propane bisdicyanamide ($[N_{111}C_3Py][DCA]_2$) and 1-trimethylammonium-3-(1-methylpiperidinium)propane bisdicyanamide ($[N_{111}C_3MPi][DCA]_2$) were synthesized and characterized by ^{1}H NMR and ^{13}C NMR. The thermal stability of these pure dicationic organics, and the density and dynamic viscosity data of pure GILs together with the binary mixture with acetonitrile, were respectively measured over the entire concentration range in the temperature range from 283.15 to 333.15 K, with 5 K intervals, at atmospheric pressure. In addition, the onset decomposition temperature (T_{onset}) and the temperature at the maximum rate of weight loss (T_{max}) were obtained. Meanwhile, thermal expansion coefficients (α) of the binary mixtures were calculated, and the temperature dependence of the viscosity of pure GILs was correlated using various empirical equations. The excess molar volume (V_m^E) and dynamic viscosity deviations ($\Delta\eta$) of the binary mixtures were respectively obtained and fitted to the Redlich–Kister (R–K) type polynomials to determine the temperature dependence of V_m^E and $\Delta\eta$. Results are discussed in terms of molecular interactions and structures to give a better understanding of these interactions between GILs and MeCN.

2 Experimental

2.1. Chemicals

High-grade (3-bromopropyl)trimethylammonium bromide ($C_6H_{15}Br_2N$), pyridine (C_5H_5N), 1-methylpiperidine ($C_6H_{13}N$), sodium dicyanamide (C_2N_3Na), silver nitrate ($AgNO_3$), acetonitrile (C_2H_3N) and ethyl acetate ($C_4H_8O_2$) were all delivered by Aladdin Industrial Inc. All materials were kept in a controlled environment to prevent moisture and contamination, and directly used without further purification. The specifications of these chemicals are presented in Table 1. Deionized water was prepared from an ultrapure water purification system (type UPR-I-5T, Ultrapure Technology Co. Ltd, China).

2.2. Synthesis and characterization

An overview of the synthesis of $[N_{111}C_3Py][DCA]_2$ and $[N_{111}C_3MPi][DCA]_2$ is depicted in Scheme 1. In order to decrease the water content in GILs, the GIL samples were constantly

Table 1 Specifications of chemicals used in this work

Chemical name	CAS no.	M.W.	Mass fraction purity	Source
Pyridine	110-86-1	79.10	>99.9%	Aladdin Industrial Inc., China
1-Methylpiperidine	626-67-5	99.17	97.0%	Aladdin Industrial Inc., China
(3-Bromopropyl)trimethylammonium bromide	3779-42-8	261.00	>99.0%	Aladdin Industrial Inc., China
Methanol	67-56-1	32.04	>99.9%	Aladdin Industrial Inc., China
Ethanol	64-17-5	46.07	>99.5%	Aladdin Industrial Inc., China
Sodium dicyanamide	1934-75-4	89.03	>96.0%	Aladdin Industrial Inc., China
Silver nitrate	7761-88-8	169.87	>99.0%	Aladdin Industrial Inc., China
Ethyl acetate	141-78-6	88.11	>99.5%	Aladdin Industrial Inc., China

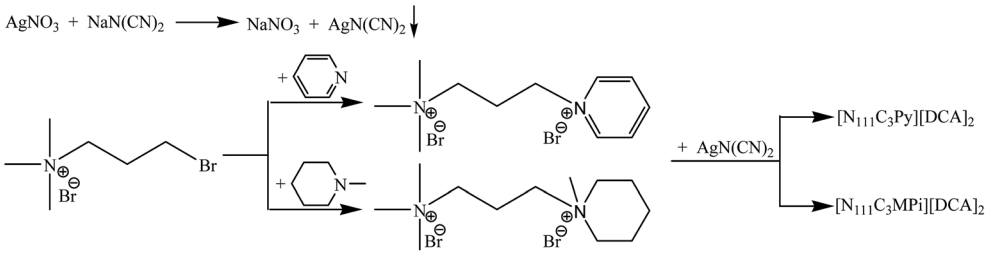

Scheme 1 Synthesis of asymmetrical ammonium-based GILs.

stored before use under a dry nitrogen atmosphere to prevent absorption of moisture and any organic contamination. The water content of the samples ($[N_{111}C_3Py][DCA]_2$ and $[N_{111}C_3MPi][DCA]_2$), measured by Karl Fischer titration technique (Aquastar V-200 Titrator, EM Science), is respectively 42 ppm and 47 ppm. Impurity levels of bromide ion in all the desired products were determined by an Oakton Ion 510 Series pH/mV/Ion/°C meter with Cole-Parmer ion specific probes (27502-05 for Br) and were lower than 10 ppm.

The structures were identified using ^{1}H NMR and ^{13}C NMR (Bruker AVANCE III 600 MHz Digital NMR Spectrometer). The NMR analysis is presented below.

$[N_{111}C_3Py][DCA]_2$. ^{1}H NMR (600 MHz, DMSO) δ 9.09 (d, J = 5.5 Hz, 2H), 8.66 (tt, J = 7.9, 1.2 Hz, 1H), 8.23 (dd, J = 7.6, 6.8 Hz, 2H), 4.66 (t, J = 7.5 Hz, 2H), 3.37 (m, 2H), 3.07 (s, 9H), 2.44 (m, 2H). ^{13}C NMR (600 MHz, DMSO) δ 146.43 (s), 145.47 (s), 128.67 (s), 119.56 (s), 62.25 (s), 58.25 (s), 52.94 (m), 24.72 (s).

$[N_{111}C_3MPi][DCA]_2$. ^{1}H NMR (600 MHz, DMSO) δ 3.36 (m, 4H), 3.31 (dd, J = 16.7, 9.7 Hz, 4H), 3.10 (s, 9H), 3.05 (s, 3H), 2.17 (m, 2H), 1.81 (m, 4H), 1.56 (m, 2H). ^{13}C NMR (600 MHz, DMSO) δ 119.57 (s), 62.49 (s), 60.80 (s), 58.85 (s), 53.00 (d, J = 3.2 Hz), 48.15 (s), 21.05 (s), 19.73 (s), 16.32 (s).

Solutions containing GIL ($[N_{111}C_3Py][DCA]_2$, $[N_{111}C_3MPi][DCA]_2$) were prepared gravimetrically using an analytical balance with a precision of ±0.1 mg (type AR224CN, Ohaus) in mass fraction by magnetic stirring. The mixtures were degassed using an ultrasonic bath to remove ubiquitous oxygen. No decomposition was observed at the experimental conditions.

2.3. Thermal stability

The thermal stability of GIL was measured using a simultaneous thermal analysis apparatus (STA 449 F3 Jupiter®, Netzsch, Germany) at a heating rate of 10 K min^{-1} in an inert atmosphere of nitrogen with a flow rate of 20 mL min^{-1}. A sample of ~10 mg was placed in a small open platinum pan and heated from room temperature to 1000 °C. The accuracy of the temperature control was found to be ±0.1 °C. The weight loss with respect to temperature was recorded. The scanning differential thermal analysis (DTA) data were obtained simultaneously with the TGA data. The observed decomposition temperatures were determined from the step tangent of the TG curves.

2.4. Density measurement

The densities (ρ) of pure GILs, MeCN and their binary mixtures were experimentally determined in the temperature range from 283.15 to 333.15 K at an interval of 5 K, employing an Anton Paar DMA 5000M digital vibrating tube densimeter automatically thermostated within ±0.01 K at ambient pressure. The accuracy and precision of the densimeter were at ±0.000005 g cm^{-3}, and the uncertainty of the measurements was estimated to be better than ±0.000001 g cm^{-3}. Before each measurement, the densimeter was calibrated at 283.15 K, 288.15 K, 293.15 K, 298.15 K, 303.15 K, 308.15 K, 313.15 K, 318.15 K, 323.15 K, 328.15 K and 333.15 K with deionized water and dry air. To reduce the uncertainties in the density values, viscosity corrections needed for GILs with highly viscous liquids are automatically made by the densimeter. Each experimental density value is the average of three measurements at each temperature. The experimental densities of MeCN were compared with the available literature data[21–25] to confirm the procedure and reproducibility of our present measurements (see Table S1 in ESI†).

2.5. Viscosity measurement

The dynamic viscosities of GILs, MeCN and their binary mixtures at atmospheric pressure from 283.15 to 333.15 K, with an interval of 5 K, were determined through an automatic microviscometer (Lovis 2000 M, Anton Paar, Graz, Austria) by using the rolling-ball principle, which is intended for determining the rolling time of a stainless steel or gold-covered ball in a liquid sample and calculating its viscosity from the rolling time. A ball rolls through a closed, liquid-filled capillary that is inclined at a defined angle. The liquid viscosity is directly related to the time obtained. Calibration was carried out by using deionized water or viscosity standard oils. The microviscometer can keep the temperature variation within ±0.01 K. This apparatus has the viscosity measurement range of 0.3–10 000 mPa s and the accuracy of up to ±0.5%. Each viscosity value is the average of three measurements at each temperature. The experimental viscosities of MeCN were compared with the literature values[21–25] (see Table S1 in ESI†).

3 Results and discussion

3.1. Thermal stability

The changes in weight and the weight loss rate of GILs with increasing temperature, at a heating rate of 10 K min^{-1}, are depicted in Fig. 1. The onset decomposition temperature (T_{onset}) and temperature at the maximum rate of weight loss (T_{max}) of the GILs are listed in Table 2. As shown in Fig. 1 and Table 2,

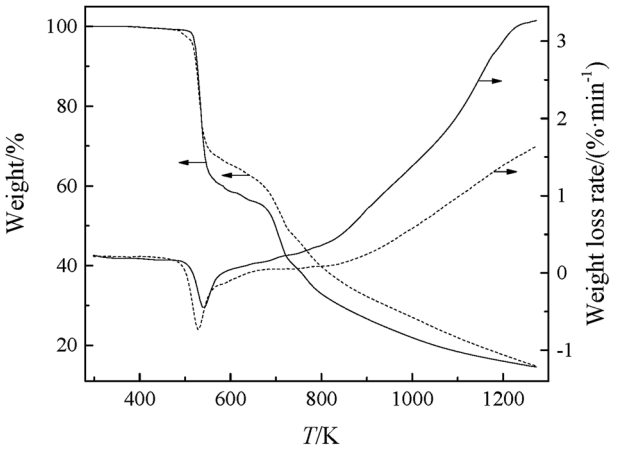

Fig. 1 TG-DTG curves of the synthesized GILs: solid line, $[N_{111}C_3Py][DCA]_2$; dashed line, $[N_{111}C_3MPi][DCA]_2$.

Table 2 Characteristic temperatures in TG-DTG curves of the GILs

GIL	T_{onset}/K	T_{max}/K
$[N_{111}C_3Py][DCA]_2$	523.12	537.89
$[N_{111}C_3MPi][DCA]_2$	514.91	525.58

these GILs are thermally more unstable than other GILs, which can be attributed to the weakly coordinating DCA anion. The thermal stabilities for the GILs increase in the following sequence: $[N_{111}C_3MPi][DCA]_2$ < $[N_{111}C_3Py][DCA]_2$, with $[N_{111}C_3Py][DCA]_2$ possessing higher thermal stability. Considering a given anion, the ILs containing $[Py]^+$ cation showed higher decomposition temperature compared with those derived from $[MPi]^+$.[26] The thermal stability determined for these GILs is in the reasonable range for various applications. As seen in Fig. 1, the TG curve for each GIL can be divided into four steps. The first step has no obvious mass loss, which shows that these GILs are thermally stable in this temperature range. The second step is the first stage of decomposition, in which the combinations of DCA anions with corresponding cationic moieties may be cleaved, for the reason that the DCA anion is a class of nucleophilic and coordinated anions, which may decompose at lower temperature, leading to corresponding mass loss.[27] The third step may be the directed cleavage of C–N bonds between the linkage group and two cationic head groups. The final step may attribute to the decomposition of carbon skeleton in the cations. It has been assumed that the thermal stability of the GILs depends on their structures and the molecular weights of cations and anions.

3.2. Density and excess volume

The densities measured for GILs, MeCN and their binary mixtures over the entire composition range at the temperatures ranging from 283.15 to 333.15 K under ambient pressure were systematically determined and are shown in Tables 3 and 4.

For pure GILs, the order of the experimental density is $[N_{111}C_3Py][DCA]_2$ > $[N_{111}C_3MPi][DCA]_2$. $[N_{111}C_3Py][DCA]_2$ has higher density value, while $[N_{111}C_3MPi][DCA]_2$ possesses lower density over the experimental temperature range. The higher value for $[N_{111}C_3Py][DCA]_2$, which contains the $[Py]^+$ cation, is due to the smaller molecular size of the cation compared with the $[MPi]^+$ cation. The densities of GILs increase with the decrease of cation molecular weight and are higher than those of the monocationic analogues reported in the literatures.[28,29] The density for $[C_3Py][DCA]$ at 298.15 K is 1.08980 g cm^{-3}, lower than that of $[N_{111}C_3Py][DCA]_2$ (1.15504 g cm^{-3}), which may be due to the stronger inter-ionic interactions of the GILs than those of the traditional monocationic ILs.[9] With the increasing temperature, densities of pure GILs were observed to linearly decrease (see Fig. S1 in ESI†) due to the decrease in the van der Waals forces, which consequently increases the mobility of the ions.[30] Molecules are farther apart from each other at higher temperatures, causing the decrease in density.

The density values of binary mixtures containing MeCN as a function of the mole fraction of GIL (x_1) at various temperatures (283.15 to 333.15) K are listed in Tables 3 and 4. As expected, the densities of binary mixtures linearly decrease with increasing temperature, while they increase with decreasing MeCN content. A linear model was consequently employed to correlate the experimental densities and temperature.[31] Volume expansion properties of GILs and their mixtures may be a prerequisite for understanding their stability in applications, especially those under higher temperature. In the present study, density changes linearly with the temperature change; the value of thermal expansion coefficient (α), a measure of how the volume changes with temperature, can be further quantified from the density data by the following expression:[32,33]

$$\alpha/K^{-1} = \left(\frac{\partial \ln V}{\partial T}\right)_p = -\frac{1}{\rho}\left(\frac{\partial \rho}{\partial T}\right)_p, \quad (1)$$

where α is the coefficient of thermal expansion in K^{-1}, V denotes the volume in cm^3, ρ is the density in g cm^{-3}, T is the thermodynamic temperature in K, and subscript p indicates constant pressure in Pa. The thermal expansion coefficients were determined as a function of temperature (see Table S2 in ESI†). The variations in the thermal expansion coefficients with temperature are not significant for the pure $[N_{111}C_3Py][DCA]_2$ and $[N_{111}C_3MPi][DCA]_2$. The values of α for pure GILs over this temperature range are in the range of 4.900×10^{-4} to 5.100×10^{-4} K^{-1}, which are similar to those of other GILs,[32] and are significantly lower than those of common organic solvents (10^{-3} K^{-1}, like MeCN) but higher than classical molten salts (1–2×10^{-4} K^{-1}). The values of α for pure GILs decrease in the following sequence: $[N_{111}C_3Py][DCA]_2$ > $[N_{111}C_3MPi][DCA]_2$. The slight increase in the value of α as the temperature increases may originate from the increase in the ordering of pure GILs. In all the binary systems ($[N_{111}C_3Py][DCA]_2$ + MeCN and $[N_{111}C_3MPi][DCA]_2$ + MeCN), the values of α all increase with the increasing concentration of MeCN and with increasing temperatures.

To attain a deeper understanding of the interaction between GIL and the organic solvent, the excess molar volume

Table 3 Experimental density (ρ), excess molar volume (V_m^E), viscosity (η), and viscosity deviation ($\Delta\eta$) of $[N_{111}C_3Py][DCA]_2$ (1) + MeCN (2) at various temperatures[a]

x_1	ρ/(g cm^{-3})	V_m^E/(cm^3 mol^{-1})	η/(mPa s)	$\Delta\eta$/(mPa s)
283.15 K				
0.0000	0.79283	0.00000	0.4012	0.0000
0.0999	0.94085	−0.97370	4.1446	−751.1908
0.1999	1.02068	−1.71560	14.1880	−1496.8373
0.2998	1.07022	−2.34740	52.8431	−2213.1164
0.3997	1.09874	−2.28366	131.4302	−2889.4636
0.4999	1.11754	−1.94751	245.2401	−3532.8549
0.6002	1.13081	−1.46086	473.5503	−4062.5019
0.7001	1.14132	−1.00940	856.9804	−4434.0060
0.7998	1.15001	−0.61026	1384.9022	−4659.5089
0.8997	1.15759	−0.30151	2374.5011	−4424.8430
1.0000	1.16399	0.00000	7557.3000	0.0000
288.15 K				
0.0000	0.78748	0.00000	0.3819	0.0000
0.0999	0.93710	−1.06971	3.7453	−384.1405
0.1999	1.01708	−1.80523	12.2943	−763.4836
0.2998	1.06687	−2.44250	42.1502	−1121.1315
0.3997	1.09560	−2.38204	97.8751	−1452.9104
0.4999	1.11432	−2.01322	174.6311	−1764.8230
0.6002	1.12773	−1.52525	321.0604	−2007.4485
0.7001	1.13827	−1.05804	553.7802	−2162.2324
0.7998	1.14706	−0.65821	848.1505	−2254.5906
0.8997	1.15467	−0.33773	1335.8011	−2154.4445
1.0000	1.16099	0.00000	3879.3002	0.0000
293.15 K				
0.0000	0.78210	0.00000	0.3641	0.0000
0.0999	0.93325	−1.16161	3.4486	−215.7600
0.1999	1.01350	−1.89961	10.7510	−427.5212
0.2998	1.06356	−2.54413	34.4992	−622.6177
0.3997	1.09248	−2.48435	75.8173	−800.1442
0.4999	1.11123	−2.09777	129.0504	−966.4130
0.6002	1.12467	−1.59225	226.4001	−1088.7837
0.7001	1.13523	−1.10687	371.2505	−1162.7783
0.7998	1.14414	−0.70962	561.9012	−1190.5347
0.8997	1.15171	−0.36192	850.2906	−1120.9892
1.0000	1.15801	0.00000	2191.0021	0.0000
298.15 K				
0.0000	0.77670	0.00000	0.3479	0.0000
0.0999	0.92940	−1.25684	3.2052	−127.5774
0.1999	1.00993	−1.99789	9.5451	−251.8027
0.2998	1.06026	−2.64942	28.7061	−363.0764
0.3997	1.08939	−2.59250	59.8222	−462.3951
0.4999	1.10809	−2.17645	98.1055	−554.9384
0.6002	1.12162	−1.66146	165.5803	−618.4203
0.7001	1.13217	−1.15193	263.8207	−650.6149
0.7998	1.14119	−0.75440	381.8602	−662.7485
0.8997	1.14879	−0.39323	561.3303	−613.7131
1.0000	1.15504	0.00000	1306.0011	0.0000
303.15 K				
0.0000	0.77127	0.00000	0.3332	0.0000
0.0999	0.92546	−1.34827	3.0028	−80.2941
0.1999	1.00637	−2.09932	8.5509	−157.7926
0.2998	1.05698	−2.75793	24.3252	−224.9822
0.3997	1.08623	−2.69155	48.2821	−283.9888
0.4999	1.10500	−2.26048	76.3252	−339.1586
0.6002	1.11858	−1.72897	125.0205	−373.7594
0.7001	1.12918	−1.20477	192.4303	−389.3130
0.7998	1.13819	−0.78296	271.0104	−393.5306
0.8997	1.14587	−0.41680	392.0407	−355.4642
1.0000	1.15211	0.00000	830.8034	0.0000
308.15 K				
0.0000	0.76581	0.00000	0.3196	0.0000
0.0999	0.92152	−1.44331	2.8266	−53.1763
0.1999	1.00283	−2.20547	7.7113	−104.0307
0.2998	1.05372	−2.87052	20.9521	−146.4733
0.3997	1.08309	−2.79382	39.6003	−183.5086
0.4999	1.10198	−2.35408	61.2755	−217.6841
0.6002	1.11555	−1.79623	96.7161	−238.1493
0.7001	1.12619	−1.25443	145.6202	−244.9286
0.7998	1.13521	−0.81098	200.1906	−245.9304
0.8997	1.14295	−0.43465	286.2104	−215.5937
1.0000	1.14921	0.00000	557.7103	0.0000
313.15 K				
0.0000	0.76032	0.00000	0.3071	0.0000
0.0999	0.91759	−1.54292	2.6723	−36.1615
0.1999	0.99930	−2.31554	7.0336	−70.3655
0.2998	1.05048	−2.98730	18.1521	−97.7738
0.3997	1.07997	−2.89941	33.2670	−121.1856
0.4999	1.09893	−2.44284	50.0027	−143.0950
0.6002	1.11256	−1.86821	76.5772	−155.1990
0.7001	1.12321	−1.30274	108.6508	−161.6527
0.7998	1.13227	−0.84251	145.4805	−163.2723
0.8997	1.14008	−0.45767	212.6704	−134.6090
1.0000	1.14634	0.00000	385.9631	0.0000
318.15 K				
0.0000	0.75479	0.00000	0.2956	0.0000
0.0999	0.91375	−1.65443	2.5404	−25.7686
0.1999	0.99579	−2.43121	6.4291	−49.9213
0.2998	1.04725	−3.10782	16.0410	−68.3228
0.3997	1.07673	−2.99083	28.2121	−84.1652
0.4999	1.09596	−2.54328	43.4605	−97.0147
0.6002	1.10959	−1.94200	63.8640	−104.7363
0.7001	1.12025	−1.35176	89.6683	−106.9457
0.7998	1.12934	−0.87169	117.5001	−107.0710
0.8997	1.13719	−0.47058	161.4022	−91.1844
1.0000	1.14350	0.00000	280.7116	0.0000
323.15 K				
0.0000	0.74922	0.00000	0.2849	0.0000
0.0999	0.90992	−1.77188	2.4252	−18.8302
0.1999	0.99229	−2.55219	5.9133	−36.3336
0.2998	1.04405	−3.23519	14.1380	−49.0794
0.3997	1.07349	−3.08442	24.1920	−59.9960
0.4999	1.09306	−2.65537	36.7422	−68.4794
0.6002	1.10664	−2.01914	51.7495	−74.5269
0.7001	1.11738	−1.41618	70.9492	−76.2975
0.7998	1.12642	−0.90043	91.6491	−76.5260
0.8997	1.13441	−0.50423	122.6207	−66.5255
1.0000	1.14068	0.00000	210.2033	0.0000
328.15 K				
0.0000	0.74362	0.00000	0.2750	0.0000
0.0999	0.90539	−1.83606	2.3240	−14.0743
0.1999	0.98889	−2.68735	5.4676	−27.0702
0.2998	1.04085	−3.36644	12.5480	−36.1132
0.3997	1.07043	−3.20431	20.9750	−43.8096
0.4999	1.09015	−2.76831	30.6054	−50.3513

Table 3 (*Contd.*)

x_1	ρ/(g cm^{-3})	V_m^E/(cm^3 mol^{-1})	η/(mPa s)	$\Delta\eta$/(mPa s)
0.6002	1.10372	−2.10255	43.2911	−53.8533
0.7001	1.11448	−1.47543	57.6375	−55.6306
0.7998	1.12358	−0.94486	73.2282	−56.1307
0.8997	1.13161	−0.53208	95.5920	−49.8901
1.0000	1.13787	0.00000	161.6706	0.0000
333.15 K				
0.0000	0.73797	0.00000	0.2658	0.0000
0.0999	0.90166	−1.97249	2.2332	−10.6614
0.1999	0.98531	−2.81029	5.0838	−20.4522
0.2998	1.03768	−3.50545	11.2140	−26.9508
0.3997	1.06739	−3.32996	18.3542	−32.4395
0.4999	1.08721	−2.87872	27.6141	−35.8462
0.6002	1.10082	−2.18985	37.5872	−38.5526
0.7001	1.11166	−1.54878	48.5280	−40.2404
0.7998	1.12080	−0.99949	60.3110	−41.0609
0.8997	1.12887	−0.56992	75.3011	−38.6997
1.0000	1.13508	0.00000	126.6806	0.0000

[a] Uncertainties are $u(T) = 0.01$ K, $u(p) = 200$ Pa, $u(x) = 0.00001$, $u(\rho) = 1 \times 10^{-5}$ g cm^{-3}, $u(\eta) = 1 \times 10^{-4}$ mPa s, $u(V_m^E) = 1 \times 10^{-5}$ cm^3 mol^{-1}, $u(\Delta\eta) = 1 \times 10^{-4}$ mPa s.

(V_m^E), expressing the extent of deviation of mixtures from ideal behavior, of the binary systems ([$N_{111}C_3$Py][DCA]$_2$ + MeCN and [$N_{111}C_3$MPi][DCA]$_2$ + MeCN) were respectively calculated from the experimental density data of the mixtures based on the following expression:[34,35]

$$V_m^E = \frac{x_1M_1 + (1-x_1)M_2}{\rho} - \left[\frac{x_1M_1}{\rho_1} + \frac{(1-x_1)M_2}{\rho_2}\right], \quad (2)$$

where ρ is the density of the mixture in g cm^{-3}, x_1 represents mole fractions of GILs in the mixture, M_1 and M_2 refer to the molecular masses of GIL and MeCN in g mol^{-1}, and V_1 and V_2 are the molar volumes of GIL and MeCN in cm^3 mol^{-1}, respectively. The calculated values of excess molar volume V_m^E for the mixtures at various temperatures are listed in Tables 3 and 4. The obtained V_m^E values of the binary system, consisting of MeCN as a function of temperature and GIL composition, are depicted in Fig. 2 and 3.

The experimental excess molar volumes can be mathematically represented by the Redlich–Kister polynomial equation:[36,37]

$$V_m^E = x_1(1-x_1)\sum_{i=0}^{3} A_i(2x_1-1)^i, \quad (3)$$

where x_1 refers to the GIL mole fraction, and A_0–A_3 denote the Redlich–Kister parameters calculated by the least-squares type algorithm. Then, the standard deviation of the fitting is defined as the following equation:

$$\sigma(V_m^E) = \left[\sum \frac{\left(V_{m\,exptl}^E - V_{m\,cal}^E\right)^2}{n-m}\right]^{0.5}, \quad (4)$$

Table 4 Experimental density (ρ), excess molar volume (V_m^E), viscosity (η), and viscosity deviation ($\Delta\eta$) of [$N_{111}C_3$MPi][DCA]$_2$ (1) + MeCN (2) at various temperatures[a]

x_1	ρ/(g cm^{-3})	V_m^E/(cm^3 mol^{-1})	η/(mPa s)	$\Delta\eta$/(mPa s)
283.15 K				
0.0000	0.79283	0.00000		
0.0999	0.93640	−1.36085		
0.2001	1.00377	−1.88498		
0.3001	1.04175	−2.05646		
0.3998	1.06511	−1.94636		
0.5002	1.08154	−1.77557		
0.6000	1.09299	−1.46325		
0.7001	1.10148	−1.06328		
0.7996	1.10806	−0.62985		
0.8998	1.11386	−0.28797		
1.0000	1.11889	0.00000		
288.15 K				
0.0000	0.78748	0.00000	0.3819	0.0000
0.0999	0.93241	−1.43318	3.9949	−750.8835
0.2001	1.00031	−1.97687	17.4160	−1494.2247
0.3001	1.03856	−2.15309	56.9202	−2209.9725
0.3998	1.06199	−2.02840	145.5904	−2874.2886
0.5002	1.07843	−1.83548	334.0607	−3444.0914
0.6000	1.09009	−1.53694	678.7513	−3853.1427
0.7001	1.09859	−1.11845	1177.0028	−4110.8998
0.7996	1.10511	−0.65109	2304.7011	−3734.6754
0.8998	1.11098	−0.30499	3991.5051	−2804.6377
1.0000	1.11602	0.00000	7552.9043	0.0000
293.15 K				
0.0000	0.78210	0.00000	0.3641	0.0000
0.0999	0.92841	−1.50767	3.6867	−446.4707
0.2001	0.99685	−2.07101	15.1392	−886.1625
0.3001	1.03541	−2.25572	45.9441	−1305.6011
0.3998	1.05881	−2.10191	111.5906	−1688.8479
0.5002	1.07538	−1.90356	243.4312	−2009.0525
0.6000	1.08720	−1.60992	465.9624	−2235.8656
0.7001	1.09568	−1.16562	729.2211	−2423.2995
0.7996	1.10223	−0.68268	1390.0052	−2210.5118
0.8998	1.10812	−0.32027	2477.2033	−1574.4559
1.0000	1.11318	0.00000	4502.8071	0.0000
298.15 K				
0.0000	0.77670	0.00000	0.3479	0.0000
0.0999	0.92442	−1.58546	3.4196	−278.5217
0.2001	0.99341	−2.16899	13.1605	−551.2202
0.3001	1.03221	−2.35320	37.6911	−808.5644
0.3998	1.05574	−2.19039	87.2882	−1039.9970
0.5002	1.07235	−1.97315	181.4506	−1228.8377
0.6000	1.08428	−1.67459	322.0602	−1369.5392
0.7001	1.09278	−1.21064	508.0509	−1465.7063
0.7996	1.09939	−0.71785	895.2501	−1358.9721
0.8998	1.10527	−0.33124	1609.8034	−926.8610
1.0000	1.11037	0.00000	2819.1027	0.0000
303.15 K				
0.0000	0.77127	0.00000	0.3332	0.0000
0.0999	0.92044	−1.66754	3.1755	−180.6008
0.2001	0.98998	−2.27102	11.6030	−356.1672
0.3001	1.02904	−2.45647	31.3811	−520.0159
0.3998	1.05280	−2.29851	69.5380	−664.9347
0.5002	1.06938	−2.05255	139.0803	−779.7539
0.6000	1.08142	−1.74937	245.8206	−856.2733
0.7001	1.08992	−1.26180	370.0421	−915.8636

Table 4 (*Contd.*)

x_1	ρ/(g cm^{-3})	V_m^E/(cm^3 mol^{-1})	η/(mPa s)	$\Delta\eta$/(mPa s)
0.7996	1.09651	−0.74075	623.1633	−845.4521
0.8998	1.10246	−0.34783	1084.9006	−567.7061
1.0000	1.10758	0.00000	1836.6025	0.0000
308.15 K				
0.0000	0.76581	0.00000	0.3196	0.0000
0.0999	0.91646	−1.75299	2.9790	−119.5863
0.2001	0.98657	−2.37770	10.3162	−234.8621
0.3001	1.02588	−2.56245	26.5041	−341.0421
0.3998	1.04978	−2.39555	56.5374	−433.0100
0.5002	1.06643	−2.13406	109.3102	−503.0946
0.6000	1.07851	−1.81241	185.3313	−549.1979
0.7001	1.08708	−1.31317	274.3805	−582.6383
0.7996	1.09376	−0.78797	449.3407	−529.4345
0.8998	1.09966	−0.36017	759.8422	−341.5472
1.0000	1.10482	0.00000	1224.0039	0.0000
313.15 K				
0.0000	0.76032	0.00000	0.3071	0.0000
0.0999	0.91247	−1.84135	2.8089	−82.9919
0.2001	0.98316	−2.48769	9.2371	−162.3142
0.3001	1.02274	−2.67330	22.7451	−234.3855
0.3998	1.04678	−2.49684	46.5810	−295.8721
0.5002	1.06356	−2.22902	86.9782	−341.3967
0.6000	1.07563	−1.88014	145.1305	−368.6528
0.7001	1.08427	−1.36878	210.1421	−389.3077
0.7996	1.09097	−0.82296	328.5107	−356.0891
0.8998	1.09690	−0.37822	544.5711	−225.7796
1.0000	1.10208	0.00000	856.1032	0.0000
318.15 K				
0.0000	0.75479	0.00000	0.2956	0.0000
0.0999	0.90850	−1.93568	2.6754	−59.3758
0.2001	0.97977	−2.60323	8.2623	−115.7300
0.3001	1.01962	−2.78885	19.6420	−166.1677
0.3998	1.04379	−2.60040	39.2504	−208.1917
0.5002	1.06058	−2.30515	70.3852	−239.1214
0.6000	1.07287	−1.96819	113.8913	−257.3102
0.7001	1.08149	−1.42703	163.4606	−269.6195
0.7996	1.08823	−0.86432	246.2922	−248.2978
0.8998	1.09416	−0.39463	399.5903	−156.9389
1.0000	1.09937	0.00000	618.4704	0.0000
323.15 K				
0.0000	0.74922	0.00000	0.2849	0.0000
0.0999	0.90452	−2.03419	2.5387	−43.6837
0.2001	0.97640	−2.72562	7.4884	−84.8095
0.3001	1.01646	−2.90347	17.3140	−120.9674
0.3998	1.04088	−2.71874	33.3481	−150.7790
0.5002	1.05761	−2.38500	58.1723	−172.1224
0.6000	1.07003	−2.04255	91.7744	−184.4120
0.7001	1.07871	−1.48556	129.8503	−192.3654
0.7996	1.08553	−0.91428	192.9417	−175.0290
0.8998	1.09146	−0.41944	302.8822	−111.1645
1.0000	1.09667	0.00000	460.1203	0.0000
328.15 K				
0.0000	0.74362	0.00000	0.2750	0.0000
0.0999	0.90054	−2.13668	2.4270	−32.8145
0.2001	0.97303	−2.85127	6.8167	−63.4963
0.3001	1.01333	−3.02380	15.3720	−89.9425
0.3998	1.03789	−2.82613	28.6281	−111.5830
0.5002	1.05465	−2.46556	48.6852	−126.6675
0.6000	1.06705	−2.08804	74.3203	−135.9640
0.7001	1.07595	−1.54452	104.9515	−140.3705
0.7996	1.08290	−0.97541	151.8803	−128.2670
0.8998	1.08877	−0.44005	233.0924	−82.1285
1.0000	1.09400	0.00000	350.2906	0.0000
333.15 K				
0.0000	0.73797	0.00000	0.2658	0.0000
0.0999	0.89656	−2.24440	2.3198	−24.8435
0.2001	0.96968	−2.98310	6.1635	−47.9780
0.3001	1.01025	−3.15277	13.6690	−67.3970
0.3998	1.03496	−2.94283	24.7680	−83.1416
0.5002	1.05162	−2.53274	41.5710	−93.3707
0.6000	1.06408	−2.13177	62.2790	−99.5333
0.7001	1.07321	−1.60246	85.5210	−103.2427
0.7996	1.08030	−1.03658	122.0300	−93.5235
0.8998	1.08610	−0.45662	182.9900	−59.5417
1.0000	1.09137	0.00000	269.5100	0.0000

[a] Uncertainties are $u(T) = 0.01$ K, $u(p) = 200$ Pa, $u(x) = 0.00001$, $u(\rho) = 1 \times 10^{-5}$ g cm^{-3}, $u(\eta) = 1 \times 10^{-4}$ mPa s, $u(V_m^E) = 1 \times 10^{-5}$ cm^3 mol^{-1}, $u(\Delta\eta) = 1 \times 10^{-4}$ mPa s.

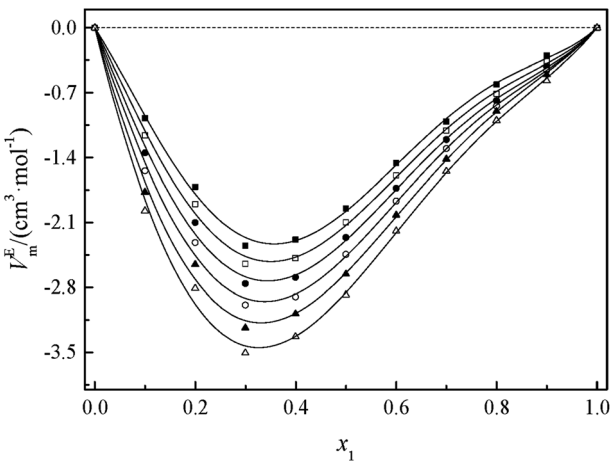

Fig. 2 Plot of excess molar volumes (V_m^E) against molar fraction (x_1) for the binary system of $[N_{111}C_3Py][DCA]_2$ (1) + MeCN(2) at various temperatures: (■) 283.15 K, (□) 293.15 K, (●) 303.15 K, (○) 313.15 K, (▲) 323.15 K, (△) 333.15 K. The solid lines represent the corresponding fittings by the Redlich–Kister equation.

where n and m refer to the number of data points and parameters, and $V_{m\ exptl}^E$ and $V_{m\ cal}^E$ represent the experimental and calculated excess molar volumes in cm^3 mol^{-1}, respectively. The coefficients of the Redlich–Kister expression as well as the standard deviations can be calculated (see Tables S3 and S4 in ESI†). Hence, the values of V_m^E of the binary system against the mole fraction were well fitted to Redlich–Kister equation, and the standard deviations of the binary mixtures are in the permissible range.

Fig. 2 and 3 show that the variation V_m^E, as a function of mole fraction of the GIL (x_1), is negative over the entire range of composition, suggesting negative deviations from ideal

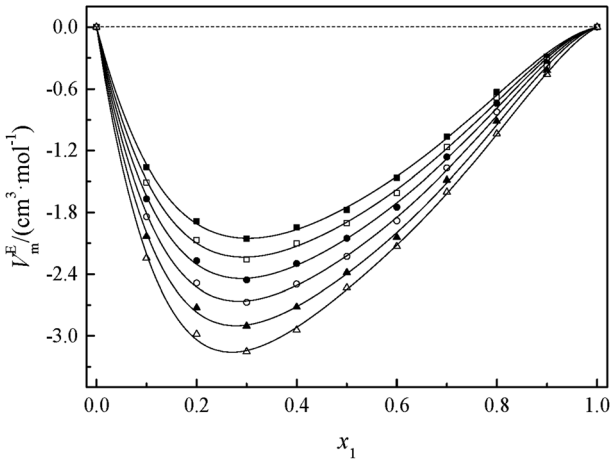

Fig. 3 Plot of excess molar volume (V_m^E) against molar fraction (x_1) for the binary system of $[N_{111}C_3MPi][DCA]_2$ (1) + MeCN(2) at various temperatures: (■) 283.15 K, (□) 293.15 K, (●) 303.15 K, (○) 313.15 K, (▲) 323.15 K, (△) 333.15 K. The solid lines represent the corresponding fittings by the Redlich–Kister equation.

solution behavior. It is more interesting that the V_m^E in every GIL + MeCN system has minimum values at around $x_1 \approx 0.3$ for all temperatures investigated, which indicates the strongest interaction. The values of V_m^E for the system consisting of GILs and relatively polar solvents may mainly depend on the following factors: (1) the dipole–dipole, ion–dipole, and ion–ion interactions between components of the binary mixtures;[21] (2) contraction or molecular packing as a consequence of differences in size and shape of molecules (free volume difference of unlike molecules);[21] (3) expansion due to the disruption of self-association in the GIL or solvent; (4) contraction owing to specific interaction between the GIL and MeCN; and (5) variation in intermolecular forces between the GIL and solvent molecules that are in contact. This behavior, negative V_m^E, can be interpreted in several opposing ways. Interactions between like molecules give rise to positive V_m^E values, while interactions between unlike molecules such as dipole–dipole interaction, dispersion force, or hydrogen bonding lead to negative contributions to V_m^E.[23] As seen in Fig. 2 and 3, the negative values of V_m^E for the mixtures over the entire investigated range of GIL mole composition and in all analyzed temperatures indicate stronger interactions between GIL and MeCN molecules than those between the pure components. The interactions between unlike molecules, $[N_{111}C_3Py][DCA]_2$, MeCN and $[N_{111}C_3MPi][DCA]_2$, MeCN, are stronger than those between MeCN molecules, and negative V_m^E values are observed with the following sequence: $[N_{111}C_3MPi][DCA]_2 > [N_{111}C_3Py][DCA]_2$. GILs can be solvated by MeCN molecules because of a strong ion–dipole interaction, resulting in weakening ion–ion interactions between anions ($[DCA]^-$) and cations in the GILs.[18,38] The packing efficiency of MeCN accommodation in the interstice of GIL networks, the difference in the interaction, and hydrogen bonding may be dominant in these binary systems. Meanwhile, the interstitial accommodation and the effect of the condensation of GIL and MeCN make further negative contributions to V_m^E. In fact, unsymmetrical curves of V_m^E may be more likely to occur while the components of the binary mixture have large molecular weight and size differences. It is observed that the curves of V_m^E are asymmetric, indicating a large molar volume difference between the two components (GIL and MeCN) of the binary mixtures.

It can be observed that values of excess molar volume for binary systems of $[N_{111}C_3Py][DCA]_2$ + MeCN and $[N_{111}C_3MPi][DCA]_2$ + MeCN decrease and become more negative with increased temperature, indicating volume expansion. The variation in V_m^E with temperature is attributed to the competition of packing efficiency and the hydrogen bonding interaction in the binary mixture. In general, as the temperature increases, the packing efficiency strengthens, leading to decrease of V_m^E value.[39] In the present binary mixtures of $[N_{111}C_3Py][DCA]_2$ + MeCN and $[N_{111}C_3MPi][DCA]_2$ + MeCN, the variation of V_m^E with temperature indicates that packing efficiency may play a dominant functional role in the change in value of V_m^E.

3.3. Viscosity and viscosity deviation

The dynamic viscosity, η, for GILs, MeCN and their binary mixtures at various temperatures over the entire concentration range from 283.15 to 333.15 K was determined (Tables 3 and 4). The viscosities are highest for the pure GIL and significantly decrease with increasing MeCN content. Meanwhile, the viscosities of the binary mixtures decrease with the increasing temperature.

The sequence for the experimental viscosities of the two pure GILs is $[N_{111}C_3MPi][DCA]_2 > [N_{111}C_3Py][DCA]_2$. Among the obtained GILs, the viscosity of $[N_{111}C_3MPi][DCA]_2$ is remarkably larger than $[N_{111}C_3Py][DCA]_2$. The viscosity may be affected by the cation's aromaticity; the aromatic compounds possess lower viscosity values than the non-aromatic ones: $[Py]^+ < [MPi]^+$. The viscosity will be greatly affected by the cation's inherent interactions related to the GIL structure and bulk distribution. The π–π interactions in pyridinium GIL were expected to provide higher resistance to shear stress due to a more rigid IL structure and bulk distribution; the results, however, showed the opposite, with lower viscosity for the pyridinium GIL, since the π–π interactions will also lend a more rigid ring structure and induce a more organized bulk distribution compared with the more flexible piperidinium ring, resulting in a relatively flexible structure and a greater entanglement of the rings in the liquid phase.[40] The viscosities of GILs are higher than those of the monocationic analogues reported in the literature.[18,41] The viscosity of the pure GILs decreases sharply at low temperature when the temperature is increased, while it decreases smoothly at high temperature (see Fig. S2 in ESI†), making the temperature-dependent viscosity of GILs challenging.

The temperature dependence of the viscosity of pure GIL ($[N_{111}C_3Py][DCA]_2$ or $[N_{111}C_3MPi]$ $[DCA]_2$) can be expressed in the following equations. A common method is by employing the three-parameter Vogel–Tammann–Fulcher (VTF) equation and modified VTF (mVTF) equation:[42]

$$\eta = Ae^{\frac{-B}{T-T_0}} \quad (5)$$

and

$$\eta = AT^{0.5}e^{\frac{-B}{T-T_0}}, \quad (6)$$

where T_0 is related to the glass temperature in K, and A and B (K) refer to adjustable parameters.

Meanwhile, other expressions, the inverse cubic equation (Litovitz equation)[43] and simple linear equation (Ghatee equation)[44] can also be used to correlate the viscosity of pure GILs with the temperature:

$$\eta = Ae^{\frac{-B}{RT^3}}, \quad (7)$$

where A is the viscosity at infinite temperature in mPa s, B is related to the activation energy of viscous flow in J K^2 mol^{-1}, and R is the universal gas constant (8.3145 J mol^{-1} K^{-1}).

$$\left(\frac{1}{\eta}\right)^{\varphi} = A + BT, \quad (8)$$

where A and B are constants characteristics of the GIL, and φ is characteristic exponent ($\varphi = 0.300$).

The equation parameters, together with correlation coefficients (R^2), can be evaluated (see Table S5 in ESI†). The results indicate that both VTF and mVTF equations can quite accurately correlate the viscosity of pure GILs with temperature. The higher accuracy of the VTF and mVTF equations may be due to the larger number of parameters in the equations.

From Tables 3 and 4, it can be observed that the values of dynamic viscosity of the binary systems decreased with the addition of MeCN, as expected. The addition of common organics with higher relative permittivity (*e.g.* MeCN) may increase the ion solvation (weakening ion–ion interactions) and result in significantly reduced viscosity of the mixture. Deviation of the viscosity, $\Delta\eta$, can be calculated from the viscosity data of the mixtures and pure components based on the following equation:[23]

$$\Delta\eta = \eta - (x_1\eta_1 + x_2\eta_2), \quad (9)$$

where η, η_1 and η_2 are respectively the dynamic viscosity of the binary mixture, pure GIL and MeCN in mPa s; x_1 and x_2 represent mole fractions of GIL and MeCN in mixture; and $\Delta\eta$ refers to deviations from a rectilinear dependence of viscosity on mole fraction. The temperature and composition dependence of viscosity deviations $\Delta\eta$ of the $[N_{111}C_3Py][DCA]_2$ + MeCN and $[N_{111}C_3MPi][DCA]_2$ + MeCN binary mixtures are listed in Tables 3 and 4 and plotted in Fig. 4 and 5. It was observed that the values of $\Delta\eta$ shown in Fig. 4 and 5 were asymmetrical and negative over the entire concentration range at each temperature for every binary mixture, exhibiting the minimum value in the GIL-rich composition region, indicating that the volume contracts upon mixing.[45] Moreover, the values of $\Delta\eta$ became less negative with increasing temperature, similar to ideal systems for the binary mixtures. Temperature plays a great influence on $\Delta\eta$, and the general tendency is to have larger deviations from ideality with decreasing temperature. On the other hand, the experimental compositions at the minimum values of $\Delta\eta$ were observed to be almost constant and independent of temperature in each mixture. Also, the values of $\Delta\eta$ for $[N_{111}C_3MPi][DCA]_2$ + MeCN are more negative at the same concentration and temperature, implying that $\Delta\eta$ became particularly strong as the cation's aromaticity in the GILs decreased.

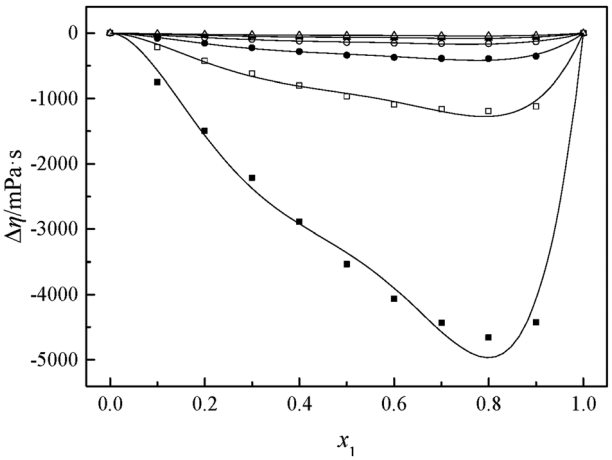

Fig. 4 Plot of viscosity deviation $\Delta\eta$ against mole fraction for the system of $[N_{111}C_3Py][DCA]_2$ (1) + MeCN (2) at different temperatures: (■) 283.15 K, (□) 293.15 K, (●) 303.15 K, (○) 313.15 K, (▲) 323.15 K, (△) 333.15 K; solid line, Redlich–Kister correlation.

The viscosity of a mixture strongly relies on the liquid's structure. Thus, $\Delta\eta$ depends on molecular interactions as well as the size and shape of the molecules. Accordingly, the viscosity deviation of a mixture containing a molecular solvent and an ionic species is the competition of molecular size and molecular interaction (H-bonds, van der Waals interactions).[46] The viscosity deviations are negative, provided that the mixture is dominated by intermolecular forces between the solute and the solvent (the van der Waals interactions). On the contrary, the viscosity deviations are positive when the mixture is dominated by strong specific interactions (H-bonds).[47] Furthermore,

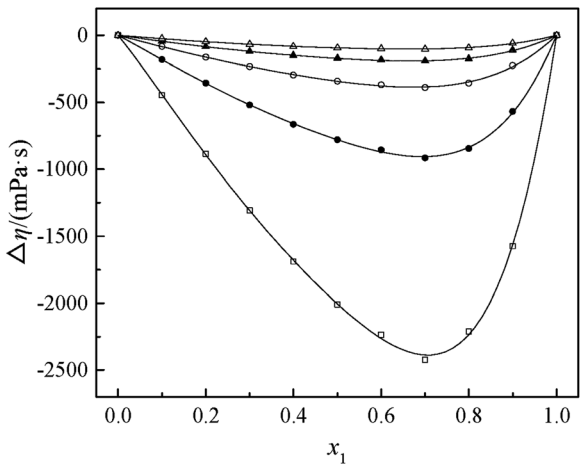

Fig. 5 Plot of viscosity deviation $\Delta\eta$ against mole fraction for the system of $[N_{111}C_3MPi][DCA]_2$ (1) + MeCN (2) at different temperatures: (□) 293.15 K, (●) 303.15 K, (○) 313.15 K, (▲) 323.15 K, (△) 333.15 K; solid line, Redlich–Kister correlation.

the negative values of $\Delta\eta$ for the binary mixtures may also imply that the viscosities of associations formed between unlike molecules are relatively greater than those of the like ones. Negative values of $\Delta\eta$ may also occur for the binary mixtures in which dispersion forces are dominant, particularly for the mixtures containing different molecular sizes.[48,49] In the present investigation, the negative values of $\Delta\eta$ showed that the interaction between cation and anion became weak owing to the solvation interaction between ions (cation and anion) and MeCN molecules. Based on the viscosity deviations shown in Fig. 4 and 5, the negative deviations can be attributed to strong van der Waals interactions and dispersion forces, and weak hydrogen bonding interaction between the molecules of GIL ($[N_{111}C_3Py][DCA]_2$, $[N_{111}C_3MPi][DCA]_2$) and MeCN.

Viscosity deviation can also be fitted to the Redlich–Kister equation:[48]

$$\Delta\eta = x_1x_2\sum_{i=0}^{3}A_i(x_1 - x_2)^i, \quad (10)$$

where x_1 and x_2 denote the mole fraction of GIL and MeCN, and A_0–A_3 refer to the Redlich–Kister parameters. Standard deviations for the viscosity calculation were obtained by eqn (11), similar to eqn (4):

$$\sigma(\Delta\eta) = \left[\sum\frac{(\Delta\eta_{exptl} - \Delta\eta_{cal})^2}{n-m}\right]^{0.5}, \quad (11)$$

where $\Delta\eta_{exptl}$ and $\Delta\eta_{cal}$ are respectively the experimental and calculated values of viscosity deviation in mPa s^{-1}; n and m refer to the number of data points and parameters. The parameters fitted to the Redlich–Kister type expression as well as the standard deviations at different temperatures over the whole composition are calculated (see Tables S3 and S4 in ESI†). It can be observed that the values of $\Delta\eta$ as a function of mole fraction were well fitted to Redlich–Kister type equation, and the standard deviations were in the permissible range.

4 Conclusions

Two ammonium-based room-temperature asymmetrical gemini ionic liquids, $[N_{111}C_3Py][DCA]_2$ and $[N_{111}C_3MPi][DCA]_2$, were synthesized and structurally characterized by ^1H NMR and ^{13}C NMR. Thermal stability was determined. Densities and dynamic viscosities for the pure GIL and binary mixture of ($[N_{111}C_3Py][DCA]_2$ + MeCN and $[N_{111}C_3MPi][DCA]_2$ + MeCN) were respectively measured over the entire composition range from 283.15 to 333.15 K under atmospheric pressure. The densities and viscosities all increase with decreasing temperature and increasing mole fraction of GIL. The values of V_m^E and $\Delta\eta$ are all negative over the entire composition range at the studied temperatures, suggesting the existence of strong self-association and weak hydrogen bonding interaction between the molecules of GIL and MeCN. The Redlich–Kister type expression was employed to correlate V_m^E and $\Delta\eta$ with the mole fraction of GIL. The investigation results are expected to be helpful for a better understanding of the fundamental physicochemical properties of asymmetrical GILs and their further industrial and academic applications.

Conflicts of interest

There are no conflicts to declare.

Acknowledgements

The present work was supported by the Science and Technology Planning Project of Henan Province (No. 162102210056), People's Republic of China.

References

1 X. Cao, L. Qiao, H. Zheng, H. Yang and P. Zhang, *RSC Adv.*, 2018, **8**, 170–175.
2 T. Ishida and H. Shirota, *J. Phys. Chem. B*, 2013, **117**, 1136–1150.
3 L. Chen, J. Chen, Z. Song, G. Cui, Y. Xu, X. Wang and J. Liu, *J. Chem. Thermodyn.*, 2015, **91**, 292–300.
4 H. Weingärtner, *Angew. Chem., Int. Ed.*, 2008, **47**, 654–670.
5 A. Corma, S. Iborra and A. Velty, *Chem. Rev.*, 2007, **107**, 2411–2502.
6 P. K. Kilaru, R. A. Condemarin and P. Scovazzo, *Ind. Eng. Chem. Res.*, 2008, **47**, 900–909.
7 P. Kilaru, G. A. Baker and P. Scovazzo, *J. Chem. Eng. Data*, 2007, **52**, 2306–2314.
8 B. Kirchner, Ionic liquids from theoretical investigations, in *Ionic Liquids*, Springer, 2010, pp. 213–262.
9 H. Shirota, T. Mandai, H. Fukazawa and T. Kato, *J. Chem. Eng. Data*, 2011, **56**, 2453–2459.
10 J. L. Anderson, R. Ding, A. Ellern and D. W. Armstrong, *J. Am. Chem. Soc.*, 2005, **127**, 593–604.
11 M. Qi and D. W. Armstrong, *Anal. Bioanal. Chem.*, 2007, **88**, 889–899.
12 K. Huang, X. Han, X. Zhang and D. W. Armstrong, *Anal. Bioanal. Chem.*, 2007, **389**, 2265–2275.
13 S. S. Bhawal, R. A. Patil and D. W. Armstrong, *RSC Adv.*, 2015, **5**, 95854–95856.
14 C. Jin, C. Ye, B. S. Phillips, J. S. Zabinski, X. Liu, W. Liu and J. M. Shreeve, *J. Mater. Chem.*, 2006, **16**, 1529–1535.
15 R. D. Rogers and K. R. Seddon, *Science*, 2003, **302**, 792–793.
16 X. Yang, H. Song, J. Wang and W. Zou, *RSC Adv.*, 2016, **6**, 29172–29181.
17 X. Yang, H. Song, J. Wang, W. Zou and J. Wu, *Korean J. Chem. Eng.*, 2015, **32**, 2369–2374.
18 Q. Zhang, Q. Li, D. Liu, X. Zhang and X. Lang, *J. Mol. Liq.*, 2018, **249**, 1097–1106.
19 R. Fareghi-Alamdari and R. Hatefipour, *J. Mol. Liq.*, 2017, **225**, 793–799.
20 S. Schneider, T. Hawkins, M. Rosander, G. Vaghjiani, S. Chambreau and G. Drake, *Energy Fuels*, 2008, **22**, 2871–2872.
21 N. Anwar and Riyazuddeen, *J. Chem. Eng. Data*, 2018, **63**, 269–289.

22 M. d. C. Grande, M. Garcia and C. M. Marschoff, *J. Chem. Eng. Data*, 2009, **54**, 652–658.
23 F. Chen, Z. Yang, Z. Chen, J. Hu, C. Chen and J. Cai, *J. Mol. Liq.*, 2015, **209**, 683–692.
24 N. Saha and B. Das, *J. Chem. Eng. Data*, 2000, **45**, 1125–1128.
25 K. Hickey and W. E. Waghorne, *J. Chem. Eng. Data*, 2001, **46**, 851–857.
26 J. A. Lazzús, *J. Mol. Liq.*, 2012, **168**, 87–93.
27 R. Fareghi-Alamdari, F. Ghorbani-Zamani and N. Zekri, *RSC Adv.*, 2016, **6**, 26386–26391.
28 J. Klomfar, M. Součková and J. Pátek, *J. Chem. Eng. Data*, 2011, **56**, 3454–3462.
29 X. Ma, J. Wei, W. Guan, Y. Pan, L. Zheng, Y. Wu and J. Yang, *J. Chem. Thermodyn.*, 2015, **89**, 51–59.
30 M. Tariq, P. Forte, M. C. Gomes, J. C. Lopes and L. Rebelo, *J. Chem. Thermodyn.*, 2009, **41**, 790–798.
31 P. D. Gyan, K. Rajiv and H. Joshi, *J. Chem. Thermodyn.*, 2014, **71**, 27–36.
32 A. S. Khan, Z. Man, A. Arvina, M. A. Bustam, A. Nasrullah, Z. Ullah, A. Sarwono and N. Muhammad, *J. Mol. Liq.*, 2017, **227**, 98–105.
33 Z. Y. Gu and J. F. Brennecke, *J. Chem. Eng. Data*, 2002, **47**, 339–345.
34 T. Peppel, M. Köckerling, M. Geppert-Rybczyńska, R. V. Ralys, J. K. Lehmann, S. P. Verevkin and A. Heintz, *Angew. Chem., Int. Ed.*, 2010, **49**, 7116–7119.
35 B. Mokhtarani, A. Sharifi, H. R. Mortaheb, M. Mirzaei, M. Mafi and F. Sadeghian, *J. Chem. Thermodyn.*, 2009, **41**, 323–329.
36 J. Wang, Y. Tian, Y. Zhao and K. Zhuo, *Green Chem.*, 2003, **5**, 618–622.
37 E. M. Živković, D. M. Bajić, I. R. Radović, S. P. Šerbanović and M. Lj. Kijevčanin, *Fluid Phase Equilib.*, 2014, **373**, 1–19.
38 N. Zec, M. Bešter-Rogač, M. Vraneš and S. Gadžurić, *J. Chem. Thermodyn.*, 2015, **91**, 327–335.
39 M. Anouti, A. Vigeant, J. Jacquemin, C. Brigouleix and D. Lemordant, *J. Chem. Thermodyn.*, 2010, **42**, 834–845.
40 A. Bhattacharjee, P. J. Carvalho and J. A. P. Coutinho, *Fluid Phase Equilib.*, 2014, **375**, 80–88.
41 L. G. Sánchez, J. R. Espel, F. Onink, G. W. Meindersma and A. B. de Haan, *J. Chem. Eng. Data*, 2009, **54**, 2803–2812.
42 O. Ciocirlan and O. Iulian, *J. Chem. Eng. Data*, 2012, **57**, 3142–3148.
43 T. A. Litovitz, *J. Chem. Phys.*, 1952, **20**, 1088–1089.
44 M. H. Ghatee, M. Zare, A. R. Zolghadr and F. Moosavi, *Fluid Phase Equilib.*, 2010, **291**, 188–194.
45 X. Li, Q. Zhou, X. Lu and S. Zhang, *J. Mol. Liq.*, 2017, **243**, 285–292.
46 M. Anouti and J. Jacquemin, *J. Chem. Eng. Data*, 2010, **55**, 5719–5728.
47 J. Chen, L. Chen and Y. Xu, *J. Chem. Thermodyn.*, 2015, **88**, 110–120.
48 S. Aznarez, M. M. E. F. de Ruiz Holgado and E. L. Arancibia, *J. Mol. Liq.*, 2016, **124**, 78–83.
49 R. J. Fort and W. R. Moore, *Trans. Faraday Soc.*, 1966, **62**, 1112–1119.